Science Bulletin 64 (2019) 802–807

Contents lists available at ScienceDirect

Science Bulletin

journal homepage: www.elsevier.com/locate/scib

Science Bulletin
www.scibull.com

Short Communication

Scatterings from surface plasmons to propagating waves at plasmonic discontinuities

Fuxin Guan [a], Shulin Sun [b,*], Shiyi Xiao [c], Qiong He [a,d], Lei Zhou [a,d,*]

[a] Key Laboratory of Micro and Nano Photonic Structures (Ministry of Education) and State Key Laboratory of Surface Physics, Fudan University, Shanghai 200433, China
[b] Shanghai Engineering Research Center of Ultra-Precision Optical Manufacturing and Department of Optical Science and Engineering, Fudan University, Shanghai 200433, China
[c] Key Laboratory of Specialty Fiber Optics and Optical Access Networks, Joint International Research Laboratory of Specialty Fiber Optics and Advanced Communication, Shanghai Institute for Advanced Communication and Data Science, Shanghai University, Shanghai 200444, China
[d] Collaborative Innovation Center of Advanced Microstructures, Nanjing 210093, China

ARTICLE INFO

Article history:
Received 18 March 2019
Received in revised form 14 April 2019
Accepted 6 May 2019
Available online 10 May 2019

Surface plasmon polaritons (SPPs) and their low-frequency counterpart spoof SPPs have attracted intensive interests in sciences [1,2], due to their unprecedented capabilities to confine electromagnetic (EM) fields at deep-subwavelength scale, leading to many applications such as super-resolution imaging [3], plasmonic lasers [4], surfaced-enhanced Raman effect [5], plasmonic waveguides [6,7] or circuits [8], etc. In practice, scatterings of SPPs to propagating waves (PWs) are inevitable as SPPs encounter discontinuities (say, interfaces between two different plasmonic systems). Such scatterings can lead to undesired radiation losses which should be avoided, especially in those applications employing SPPs as information carriers (say, plasmonic waveguides and nano-circuits [6–8]). Meanwhile, SPP-PW scatterings can also be utilized to achieve certain desired functionalities. For example, one can purposely place a set of carefully designed scatters on a plasmonic surface to scatter SPPs, generating fascinating effects such as holograms, focusing, or even directional radiations [9,10]. However, theoretical understandings on the inherent physics governing SPP-PW scatterings are far from satisfactory. Without a simple picture on such processes, people usually have to rely on full-wave simulations to optimize the devices to either suppress or utilize the SPP-PW scatterings. Although several theoretical approaches were proposed to study the SPP transmission/reflection behaviors at certain plasmonic interfaces [11,12], the SPP-PW scatterings are usually overlooked. Moreover, since PWs have infinite channels to transport in free space, it is difficult to derive an analytical formula to describe such SPP-PW processes.

In this work, we derive a simple but intuitive analytic model to describe the SPP-PW scatterings at plasmonic discontinuities in certain scenarios. Via thoroughly analyzing the SPP-PW scatterings at the interface between two three-dimensional (3D) plasmonic metals with distinct properties, we find that while the re-emissions to PWs from the SPP fields with vertical polarization suffer from strong screenings by the plasmonic materials, those contributed by SPP fields with tangential polarization do not. Such observations motive us to propose a charge-density-wave (CDW) model to analytically study the SPP-PW scatterings at the discontinuity of 2D plasmonic systems only supporting tangentially-polarized SPPs. Our analytical model is not only justified by full wave simulations in ideal model systems, but has also been used to predict how to efficiently manipulate the SPP-PW processes in 2D plasmonic junctions, which may find useful applications in practice (e.g., in near-field microscopy and imaging, plasmonic circuits, holography, etc.).

We start from studying a model system schematically depicted in Fig. 1, which is a plasmonic junction connecting two semi-infinite 3D plasmonic metals (with permittivity given by ε_1 and ε_2, respectively) at $x = 0$. Assume that an SPP beam with unitary amplitude propagates along the x direction and strikes at such plasmonic interface. In addition to the reflected and transmitted SPP beams (with coefficients r_{SPP} and t_{SPP}, and wave-vectors k^{I}_{SPP}, k^{II}_{SPP}, respectively) flowing on the xy surface, there must also be scattered PWs in the free space (Fig. 1), which is the key issue to be addressed here. To investigate the SPP-PW scatterings, we first employ finite-element-method (FEM) simulations to study the model depicted in Fig. 1, with $\varepsilon_1 = -1.12$ fixed but with ε_2 changed continuously. As an example, we depict in Fig. 2b the FEM-simulated H_y field pattern in the plasmonic junction with $\varepsilon_2 = -16$. Obviously, as the SPP

SPECIAL TOPIC: Electromagnetic Metasurfaces: from Concept to Applications.

* Corresponding authors.
E-mail addresses: sls@fudan.edu.cn (S. Sun), phzhou@fudan.edu.cn (L. Zhou).

https://doi.org/10.1016/j.scib.2019.05.003
2095-9273/

beam strikes at the interface located at $x = 0$, transmission and reflection of SPP can happen, which have been thoroughly studied in previous literature [13]. Moreover, we also find considerable scatterings to the far-field PW channels (see Fig. 2b, c). To illustrate the key features of such scatterings, we plot in the inset of Fig. 2b the calculated scattering angular distribution, with $\varphi_p = 25.1^\circ$ and $\Delta\varphi = 71.1^\circ$ denoting the peak radiation angle and the bandwidth of the radiation pattern, respectively. Changing ε_2 to –1.8,

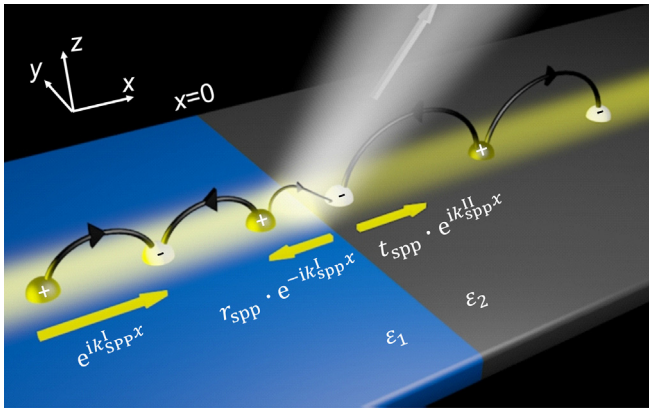

Fig. 1. Schematic of two different semi-infinite plasmonic metals (denoted as ε_1 and ε_2) jointed at $x = 0$. While the SPPs propagate along +x direction, they are transformed into three channels, i.e., reflection, transmission and radiations. Here, r_{SPP}, t_{SPP} denote the reflection and transmission coefficients of SPPs, respectively.

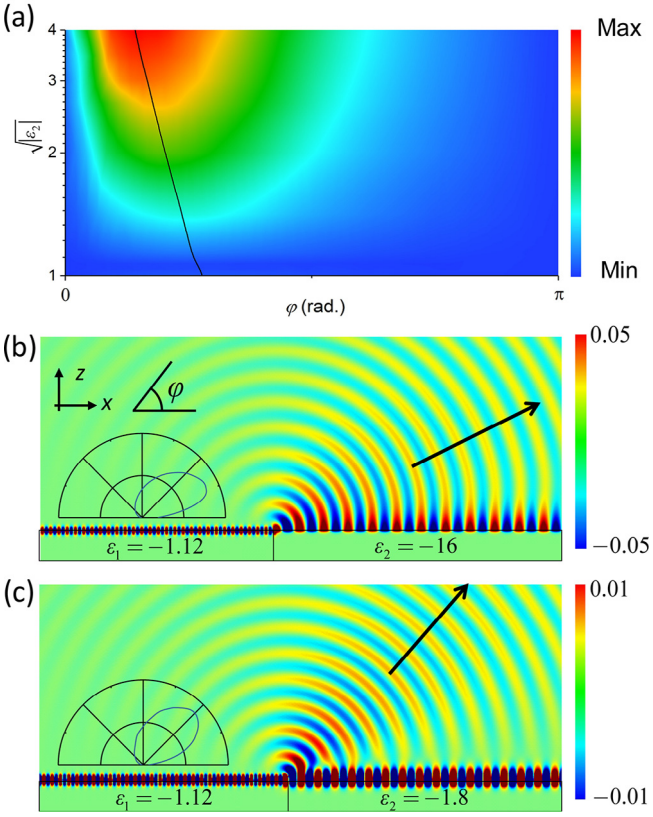

Fig. 2. Phase diagram and full-wave simulations of SPP-PW scattering. (a) FEM simulated scattering far-field intensity (color map) as function of φ (radiation angle) and ε_2 when an SPP strikes at the boundary of two plasmonic metals. The black solid line depicts the peak radiation angle φ_p in various ε_2 with ε_1 fixed at –1.12. We choose two different cases from (a) to plot the H_y field distribution inside the plasmonic junction systems with $\varepsilon_2 = -16$ (b) and $\varepsilon_2 = -1.8$ (c), respectively. It is clear that the peak radiation angle of the scattering far-field can be largely tuned by changing ε_2.

we find that the scattered field becomes weaker since the difference between two plasmonic metals gets smaller (Fig. 2c). More importantly, the radiation peak angle changes accordingly. To get a comprehensive picture on such SPP-PW scatterings, we plot in Fig. 2a the field intensity of the scattered field versus φ and ε_2, showing that the scattering pattern can indeed be continuously tuned by varying ε_2. Obviously, these interesting SPP-PW scattering properties are closely related to the wave-vectors of SPP modes in two metals, dictated by ε_1 and ε_2, respectively.

We now try to establish an analytical model to quantitatively describe such SPP-PW processes. We note that the far-field scatterings are ultimately caused by oscillating currents (serving as the secondary radiation sources) generated in the plasmonic system, which can be computed through $\vec{j}(\vec{r}) = -i\omega[\varepsilon(\vec{r}) - \varepsilon_0]\vec{E}_{local}(\vec{r})$. However, the local electric fields $\vec{E}_{local}(\vec{r})$, including not only the incident SPP fields but also the scattered fields to both SPP channels (the reflection and transmission of SPP) and PW channels, are difficult to know before we have solved the whole problem self-consistently. In the lowest order approximation, we neglect the PW contributions to the local fields, and thus we assume that $\vec{E}_{local}(\vec{r})$ only contains contributions from the SPP fields. Therefore, current in metal I is a sum of those fields associated with the incident SPP and the reflected SPP ($\vec{j} = \vec{j}_{in} + \vec{j}_{r}$), while that in metal II is solely determined by the transmitted SPP ($\vec{j} = \vec{j}_{t}$). Noting that SPP field decays quickly to zero as leaving the surface, we can further approximate each of such bulk current as a surface current sheet with a form of $\vec{J}(\vec{r},t) = \vec{J}e^{ik_{SPP}x}e^{-iwt}\delta(z)$ where $\vec{J} = (J^x\hat{x} + J^z\hat{z})$ represents a surface SPP source current [14]. The amplitude of such surface current is related to that of the bulk current through $\vec{J}(\vec{r},t) = \vec{j}(\vec{r},t)/\alpha_m$, where $\alpha_m = \sqrt{(k_{SPP})^2 - \varepsilon_m(k_0)^2}$ denotes the SPP decay rate in metal. The final current source in such a model system can thus be written as:

$$\vec{J}(\vec{r}) = \left[\left(\vec{J}_{in}e^{ik^{I}_{SPP}\cdot x} + \vec{J}_{r}e^{-ik^{I}_{SPP}\cdot x}\right)\theta(-x) + \vec{J}_{t}e^{ik^{II}_{SPP}\cdot x}\theta(x)\right]\delta(z), \quad (1)$$

where $\theta(x) = \begin{cases} 1 & x \geq 0 \\ 0 & x < 0 \end{cases}$ is a step function, $\vec{J}_{in}$, $\vec{J}_{t}$ and $\vec{J}_{r}$ are the strengths of the surface SPP sources generated by the incident, transmitted and reflected SPP beams, respectively. We now analytically study the radiations of the current source given in Eq. (1), starting from examining one component of Eq. (1), i.e., a semi-infinite surface SPP source,

$$\vec{J}(\vec{r}) = \vec{J}_{in}e^{ik_{SPP}x}\theta(-x)\delta(z). \quad (2)$$

It is well accepted that an infinite-long ideal surface SPP source $\vec{J}_{in}e^{ik_{SPP}x}\delta(z)$ cannot radiate to the free space, since the interferences of radiations from different parts of the source will form a beam with tangential wave-vector $k_x = k_{SPP} > k_0$, sharing the same physics as that in the Cherenkov radiation [15]. However, such an argument does not hold for a truncated surface SPP source for which the interferences are not complete to form an evanescent wave, especially at the vicinity of $x = 0$, where no SPP source currents are available in the $x > 0$ region. Therefore, strong radiations must happen at the vicinity of $x = 0$, due to such incomplete interferences. We now analytically derive the radiation field of the semi-infinite surface SPP source (Eq. (2)). The field radiated from any current source can be analytically calculated by [14]

$$\vec{E}(\vec{r},\omega) = i\mu_0\omega\int \overleftrightarrow{G}(\vec{r},\vec{r}';\omega)\cdot\vec{J}(\vec{r}')d\vec{r}', \quad (3)$$

where $\overleftrightarrow{G}(\vec{r},\vec{r}';\omega)$ is the dyadic Green's function in frequency domain. Put Eqs. (2) into (3), we can obtain the scattered field

$\vec{E}(\vec{r},\omega)$ by analytically performing the integration in Eq. (3), based on the technique developed in Ref. [14]. Specifically, under the far-field condition, we have (see Supplementary Section 1)

$$\vec{E}_{\rm far}(r,\varphi) = -\frac{\mu_0\omega e^{i(k_0 r-\pi/4)}}{i\sqrt{8\pi k_0 r}(k_{\rm SPP}-k_0\cos\varphi)}(J^x_{\rm in}\sin\varphi - J^z_{\rm in}\cos\varphi)\hat{e}_\varphi, \quad (4)$$

where the two terms inside the bracket are contributed by the *x*- and *z*-polarized surface currents, respectively. Eq. (4) tells us all information of the scattering patterns. Considering the radiation contributed by the ***x***-polarized surface current, we can straightforwardly derive (from the first term in the bracket of Eq. (4)) the following expressions to describe the peak angle and the bandwidth of the radiation:

$$\begin{cases} \varphi_{\rm peak} = \cos^{-1}(k_0/k_{\rm SPP}), \\ \triangle\varphi = \left|\cos^{-1}\left[\frac{\sqrt{3}k_{\rm SPP}+2k_0}{2k_{\rm SPP}+\sqrt{3}k_0}\right] - \cos^{-1}\left[\frac{2k_0-\sqrt{3}k_{\rm SPP}}{2k_{\rm SPP}-\sqrt{3}k_0}\right]\right|. \end{cases} \quad (5)$$

Eq. (5) reveals that the key properties of the radiations are dictated by the ratio $k_{\rm SPP}/k_0$. As $k_{\rm SPP}$ increases from k_0 to ∞, $\varphi_{\rm peak}$ changes from 0° to 90°, indicating that scatterings turn to the direction more perpendicular to the *xy*-plane. Inversion symmetry tells us that if the SPP travels along –*x* direction, $\varphi_{\rm peak}$ must change from 180° to 90° as $|k_{\rm SPP}|$ increases. Meanwhile, the bandwidth of the radiation peak $\triangle\varphi$ also monotonically increases with increasing $|k_{\rm SPP}|$. Such a tendency can be clearly seen by checking two extreme cases in Eq. (5): $\triangle\varphi$ turns to 0 as $k_{\rm SPP}$ decreases to k_0 but reaches $2\pi/3$ as $k_{\rm SPP}$ approaches ∞.

Similarly, for the radiation contributed by the *z*-polarized surface current (the second term in the bracket of Eq. (4)), we find that

$$\begin{cases} \varphi_{\rm peak} = 0, \\ \triangle\varphi = 2\cos^{-1}\left[\frac{k_{\rm SPP}}{2k_{\rm SPP}-k_0}\right]. \end{cases} \quad (6)$$

An important difference between Eqs. (6) and (5) is that the radiation peak is always at the angle 0°, dictated by the vertical polarization of the source. Meanwhile, $\triangle\varphi$ exhibits a similar behavior as that in the *x*-polarized case.

With the radiation properties of a single semi-finite SPP source current fully understood, we now use our model to study the SPP-PW scatterings in the plasmonic junction. Obviously, the radiation fields are now contributed by three semi-infinite SPP surface currents generated by the incident, reflected and transmitted SPPs, respectively. Therefore, the total radiation field is given by (see Supplementary Section 2):

$$\begin{aligned} \vec{E}_{\rm total}(r,\varphi) = {} & \vec{E}_0(r)\cdot\left(\frac{J^x_{\rm in}\sin\varphi}{k^{\rm I}_{\rm SPP}-k_0\cos\varphi} - \frac{J^x_{\rm r}\sin\varphi}{k^{\rm II}_{\rm SPP}-k_0\cos\varphi} + \frac{J^x_{\rm t}\sin\varphi}{k^{\rm I}_{\rm SPP}+k_0\cos\varphi}\right) \\ & - \vec{E}_0(r)\cdot\left(\frac{J^z_{\rm in}\cos\varphi}{k^{\rm I}_{\rm SPP}-k_0\cos\varphi} - \frac{J^z_{\rm r}\cos\varphi}{k^{\rm II}_{\rm SPP}-k_0\cos\varphi} + \frac{J^z_{\rm t}\cos\varphi}{k^{\rm I}_{\rm SPP}+k_0\cos\varphi}\right), \end{aligned} \quad (7)$$

where $\vec{E}_0(r) = -\frac{\mu_0\omega}{i\sqrt{8\pi k_0 r}}e^{i(k_0 r-\pi/4)}\hat{e}_\varphi$.

We take a particular plasmonic junction system (see Fig. 1a) to benchmark our theory, which contains two plasmonic metals with their permittivities given by $\varepsilon_1 = 1-(\omega_{\rm p}/\omega)^2$, $\varepsilon_2 = 1-\left(\tilde{\omega}_{\rm p}/\omega\right)^2$ with $\tilde{\omega}_{\rm p} = \omega_{\rm p}/\sqrt{3}$. Without losing generality, we assume that the working frequency is $\omega = \omega_{\rm p}/3$, and thus the wave-vectors of SPPs at two plasmonic metals are $k^{\rm I}_{\rm SPP} = 1.06k_0$ and $k^{\rm II}_{\rm SPP} = 1.41k_0$, respectively. Assuming that an SPP beam is launched on metal I and strikes at the interface, we can easily employ the single-mode approximation following the theory developed in Ref. [13] to obtain $t_{\rm SPP}$ and $r_{\rm SPP}$, which connect the *z*-polarized of incident SPP electric field with those of transmitted and reflected ones at the ($x = 0$, $z = 0$) position. With $t_{\rm SPP}$ and $r_{\rm SPP}$ known, we can analytically derive $J^x_{\rm t}$ and $J^x_{\rm r}$ as (see more details and their *z*-components in Supplementary Section 2)

$$\begin{cases} J^x_{\rm t} = \left(k^{\rm I}_{\rm SPP}/k^{\rm II}_{\rm SPP}\right)t_{\rm SPP}J^x_{\rm in}, \\ J^x_{\rm r} = -r_{\rm SPP}J^x_{\rm in}. \end{cases} \quad (8)$$

With all parameters known, we put $\vec{J}_{\rm t}$ and $\vec{J}_{\rm r}$ into Eq. (7) to calculate the angular distributions of radiated power flow, normalized against that power flow carried by the incident SPP wave, and depicted the results as the blue dashed line in Fig. 3a.

We next employ FEM simulations to benchmark our analytical theory. Fig. 3a compares the radiation patterns calculated by our theory (blue dashed line) and FEM simulations (red solid line). Significant differences are found between these two results, especially in the small-angle region. To see more clearly the origins of such discrepancies, we use FEM simulations to separately compute radiations patterns caused by total *x*- and *z*-polarized currents, and then compare them with those calculated by the analytical theory in Fig. 3b and c, respectively. Distinct behaviors are noted in two different cases. Whereas our theory can reasonably predict the general behaviors of the SPP-PW scatterings contributed by the *x*-polarized current (Fig. 3b), it completely fails for the case of *z*-polarized current, as shown in Fig. 3c. Such distinct results motivate us to re-examine the validities of our initial assumption, that is, the current source is solely determined by the SPP field. Fig. 3d and e schematically depict the radiation properties of an array of *x*-polarized and *z*-polarized SPP dipole sources, respectively. In the former case, re-emissions of SPP fields to the in-plane directions (i.e., $\varphi = 0°, 180°$) are essentially zero so that their contributions to the local-field corrections inside the metals are also negligible. However, in the latter case, the re-emissions from SPP sources to the in-plane directions can significantly alter the "local" fields inside the media, making our initial assumption invalid. Such pronounced self-screening effects well explained why the developed model fails to quantitatively describe the SPP-PW scatterings contributed by the *z*-polarized SPP currents. Certain discrepancies still exist between our theory and full-wave simulations even for the case of *x*-polarized source (see Fig. 3b). We find that they are not caused by the applications of single-mode approximation, but rather due to another approximation adopted here, i.e., neglecting the emissions from the near-fields generated at the plasmonic discontinuity (see Supplementary Section 3).

The above discussions revealed that our analytical model is particularly suitable to study the SPP-PW scatterings in those systems where the induced current only has a tangential polarization. Obviously, 2D materials (e.g., graphene and 2D electron gas) and highly anisotropic systems (e.g., hyperbolic metamaterials) satisfy this requirement, since they typically do not exhibit *z*-polarized responses. In what follows, we will employ our theory to study the SPP-PW scatterings at plasmonic junctions involving these systems.

We first study an ideal system consisting of a truncated 2D system, as shown in Fig. 4a. In this case, the transmitted SPP source current $J^x_{\rm t}$ equals to 0, and thus we only need to obtain the reflected SPP current $J^x_{\rm r}$, and then use Eq. (7) (setting the *z*-polarized currents zero) to study the SPP-PW scattering properties in such a system. Specifically, we first analyze the SPP dispersions of an ideal system without boundary. Assuming that the surface conductivity of the system under study is given by $\sigma(\omega) = \frac{ie^2 v_{\rm f}\sqrt{n}}{\hbar\sqrt{\pi}(\omega+i\Gamma)}$, where $v_{\rm f} = 9\times10^5$ m/s is the Fermi velocity, $n = 5\times10^{11}$ cm^{-2} is the electron density and $\Gamma = 0$ THz is the damping rate (we neglect the losses at the moment), we use $k_{\rm SPP} = k_0\cdot\sqrt{1-4\varepsilon_0/(\mu_0\sigma^2)}$ [16] to compute the dispersion of SPP in such system, and depict the results in Fig. 4d. We now choose two frequencies, 0.12 and 0.74 THz, to study the SPP-PW scattering patterns at the truncated system, through both FEM simulations and our analytical theory. As shown in Fig. 4g, in both cases our theoretical predictions are

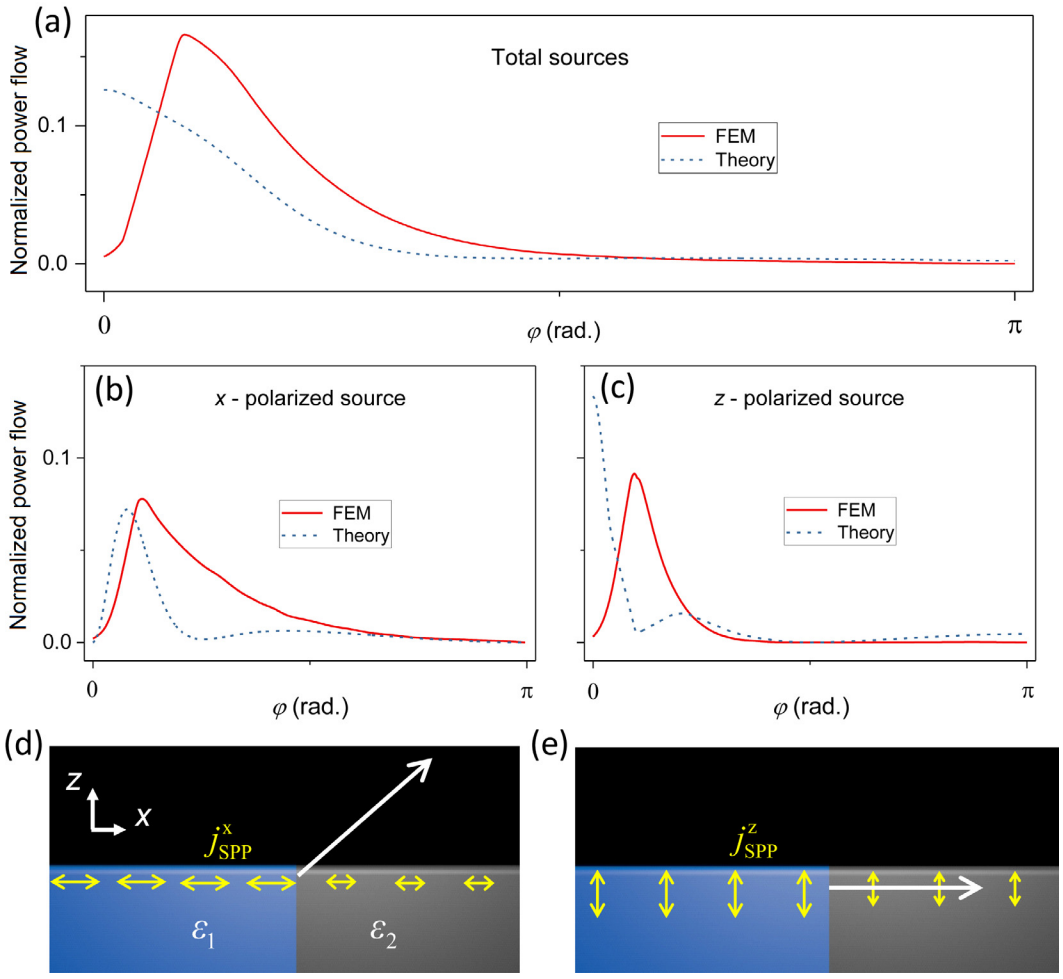

Fig. 3. Verifications of our theory in 3D plasmonic system. (a–c) The normalized SPP scattering far-field power flow angular distribution of an arbitrary plasmonic junction system ($\varepsilon_1 = 1 - (\omega_p/\omega)^2$, $\varepsilon_2 = 1 - \left(\tilde{\omega}_p/\omega\right)^2$ with $\tilde{\omega}_p = \omega_p/\sqrt{3}$) at an arbitrary frequency $\omega = \omega_p/3$, computed via full wave simulations (red line, with all source currents considered) and our theoretical model (blue dashed line, with only SPP source current considered). In (a), both *x* and *z* polarized source currents are considered. In (b, c), the contributions of *x* and *z* polarized source current are individually discussed. (d, e) Schematics of radiations of *x* and *z* polarized source currents in the plasmonic junction system, with a strong self-screening effect existing in *z* polarization case (e).

in quantitative agreement with the corresponding FEM simulations, thanks to the absence of the *z*-polarized source current. Moreover, we find that the scattering patterns at two frequencies are quite different. At 0.12 THz where k_{SPP} is only $1.1k_0$, we find that both the peak radiation angle and bandwidth are relatively small (26.3° and 59.3°, respectively). Meanwhile, at 0.74 THz, both the peak radiation angle and the bandwidth obviously increase (78.5° and 92.2°, respectively), simply because now $k_{SPP} = 3k_0$ becomes much larger. These behaviors are consistent with our theory (see Eq. (5)).

Our theory can also be employed to study the SPP-PW scatterings in realistic 2D plasmonic systems. As shown in Fig. 4b, we first study the scatterings of SPPs to PWs at the boundary of a semi-infinite graphene with $v_f = 9 \times 10^5$ m/s, $\Gamma = 0.51 f_0$, $n = 9.04 \times 10^{11}$ cm^{-2} [17]. From Fig. 4e where the dispersion of SPP is depicted, we find that while $\mathrm{Re}(k_{SPP})$ is much larger than k_0 in most cases, $\mathrm{Im}(k_{SPP})$ is also considerable and cannot be neglected. Following similar computational strategy, we adopted our theory to study the SPP scatterings in such system at two frequencies (5.8 and 7.8 THz). Again, the analytical results agree well with simulations (see Fig. 4h). A unique feature of such scatterings is that the peak radiation angle is always around $\varphi = 90°$, since in graphene we always have $\mathrm{Re}(k_{SPP}) >> k_0$, thanks to the extraordinary subwavelength field confinement capability of graphene [16].

Finally, we employ our theory to study the SPP-PW scatterings in a 2D meta-plasmonic system, which is a semi-infinite metallic mesh (with lattice constant *a*), as depicted in Fig. 4c. At the wavelength regime satisfying $\lambda >> a$, such a system can be regarded as a 2D plasmonic medium supporting spoof SPPs at microwave frequencies. In particular, such a system does not exhibit perpendicular susceptibility, which is precisely the desired medium for which our theory is applicable. Fig. 4f shows the dispersion relation of spoof SPP on the system (with infinite size), calculated by FEM simulations. Again, we choose two arbitrary frequencies (8.50 and 19.1 GHz) to study the SPP-PW scattering properties on such a system, with both FEM simulations and our theory. Fig. 4i compares the results obtained by two approaches. We find that our theory has indeed captured the essential features of the SPP-PW scatterings in such systems. Moreover, we note that in such a system the peak angles and bandwidths of the SPP-PW scatterings are always significantly smaller than those in graphene case, simply because here the SPP wave-vectors are not very large.

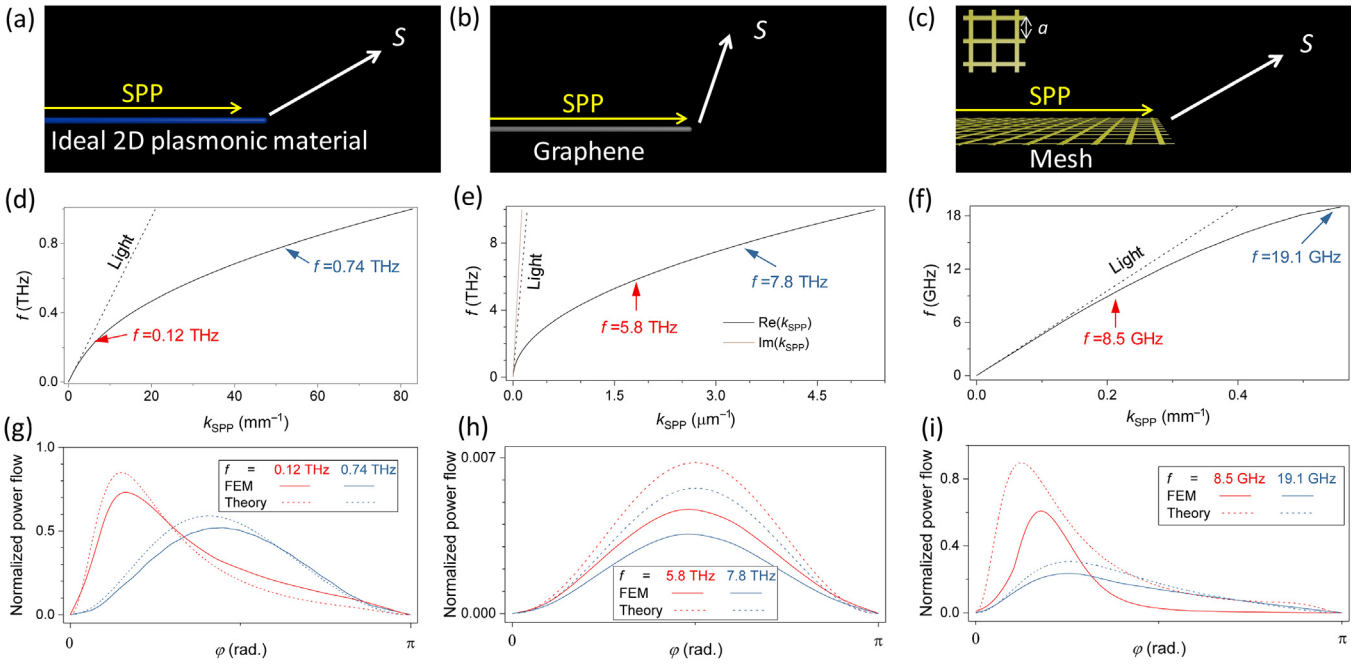

Fig. 4. Verifications of our theory in 2D plasmonic systems, including an ideal semi-infinite 2D plasmonic system (a), semi-infinite graphene (b) and artificial metasurface composed of a single layer of metallic mesh with the periodicity of $a = 5$ mm and the wire width of 0.1 mm (c). The calculated SPP dispersion relations and representative normalized scattering far-field power flow distributions of three 2D systems are depicted in (d–f) and (g–i), respectively. In (g), since the far-field radiation is relatively weak at 0.74 THz ($k_{SPP} = 3k_0$) due to a large SPP reflection in comparison with 0.12 THz ($k_{SPP} = 1.1k_0$), the normalized power flow is multiplied by 5 for a clearer view (blue lines). In (e, h), at 5.8 and 7.8 THz, the SPP eigen wavevectors of graphene are $k_{SPP} = (15 + 0.61i)k_0$ and $k_{SPP} = (20 + 0.62i)k_0$, whose imaginary parts represent SPP damping effect in graphene. In (f, i), at 8.5 and 19.1 GHz, the SPP eigen wavevectors are $k_{SPP} = 1.08k_0$ and $1.4k_0$, respectively.

In summary, via analyzing the SPP-PW scatterings at 3D plasmonic junctions, we find that the re-emissions to free-space PWs of SPP currents with tangential polarization does not suffer from significant self-screening effect but the same is not true for another polarization. Such a unique feature stimulates us to establish a simple analytical model to study the complicated SPP-PW scatterings in junctions involving plasmonic materials with tangential responses only. Our theory is well justified in various realistic plasmonic junctions involving 2D materials (graphene) and metaplasmonic system, where the peak angles and angular bandwidths of SPP-PW scatterings are found to strongly depend on the wavevectors of the (spoof) SPPs supported by the 2D plasmonic systems. Our work provides a simple way to understand and control the scatterings of SPPs to the free space, which are important in many SPP related applications.

Conflict of interest

The authors declare that they have no conflict of interest.

Acknowledgments

This work was financially supported by National Key Research and Development Program of China (2017YFA0303500 and 2017YFA0700201), National Natural Science Foundation of China (11734007, 11874118, 11674068, 91850101, 11704240, and 11474057), Shanghai Science and Technology Committee (16ZR1445200, 16JC1403100, 18ZR1403400, 17ZR1409500 and 18QA1401800), Shanghai East Scholar Plan and Fudan University-CIOMP Joint Fund.

Author contributions

F. Guan performed theoretical calculations. Q. He and S. Xiao helped to analyze the data. S. Sun and L. Zhou supervised the project and wrote the manuscript. All authors discussed the results and commented on the manuscript.

Appendix A. Supplementary data

Supplementary data to this article can be found online at https://doi.org/10.1016/j.scib.2019.05.003.

References

[1] Raether H. Surface plasmons on smooth and rough surfaces and on gratings. Springer tracts in mordern physics; 1988. p. 111.
[2] Barnes W, Dereux A, Ebbesen T. Surface plasmon subwavelength optics. Nature 2003;424:824–30.
[3] Fang N, Lee H, Sun C, et al. Sub-diffraction-limited optical imaging with a silver superlens. Science 2005;308:534–7.
[4] Oulton RF, Sorger VJ, Zentgraf T, et al. Plasmon lasers at deep subwavelength scale. Nature 2009;461:629–32.
[5] Nie S, Emory SR. Probing single molecules and single nanoparticles by surface-enhanced Raman scattering. Science 1997;275:1102–6.
[6] Bozhevolnyi SI, Volkov VS, Devaux E, et al. Channel plasmon subwavelength waveguide components including interferometers and ring resonators. Nature 2006;440:508–11.
[7] Fu Y, Hu X, Lu C, et al. All-optical logic gates based on nanoscale plasmonic slot waveguides. Nano Letts 2012;12:5784–90.
[8] Wei H, Wang Z, Tian X, et al. Cascaded logic gates in nanophotonic plasmon networks. Nat Commun 2011;2:387–91.
[9] Ozaki M, Kato J, Kawata S, et al. Surface-plasmon holography with white-light illumination. Science 2011;332:218–20.
[10] Chang CM, Chu CH, Tseng ML, et al. Light manipulation by gold nanobumps. Plasmonics 2012;7:563–9.
[11] Stockman MI. Slow propagation, anomalous absorption, and total external reflection of surface plasmon polaritons in nanolayer systems. Nano Lett 2006;6:2604–8.
[12] Oulton RF, Pile DFP, Liu Y, et al. Scattering of surface plasmon polaritons at abrupt surface interfaces: implications for nanoscale cavities. Phys Rev B 2007;76:035408.
[13] Guan F, Sun S, Ma S, et al. Transmission/reflection behaviors of surface plasmons at an interface between two plasmonic systems. J Phys: Condens Matter 2018;30:114002.
[14] Grüner G. The dynamics of charge-density waves. Rev Mod Phys 1988;60:1129–81.

[15] Sun S, He Q, Xiao S, et al. Gradient-index meta-surfaces as a bridge linking propagating waves and surface waves. Nat Mater 2012;11:426–31.
[16] Jablan M, Buljan H, Soljačić M, et al. Plasmonics in graphene at infrared frequencies. Phys Rev B 2009;80:245435.
[17] Miao Z, Wu Q, Li X, et al. Widely tunable terahertz phase modulation with gate-controlled graphene metasurfaces. Phys Rev X 2015;5:041027.

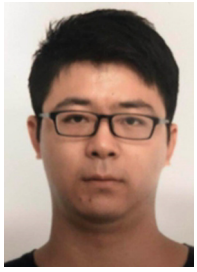

Fuxin Guan is a Ph.D. candidate in Physics Department of Fudan University. His research interest focuses on understanding and manipulating the surface plasmon transmission and reflection as well as the scattering from surface plasmons to propagating waves in various three-dimensional or two-dimensional plasmonic systems.

Shulin Sun received his Ph.D. degree in Physics Department of Fudan University in 2009. From 2010 to 2013, he was a postdoctoral fellow of the Physics Division of National Center for Theoretical Sciences in Taiwan University. In 2013, he joined Department of Optical Sciences & Engineering of Fudan University as an associate professor. His research fields include metamaterial/metasurface, plasmonics, and photonic crystals.

Lei Zhou received his Ph.D. degree in Physics from Fudan University in 1997. From 1997 to 2000, he was a postdoctoral fellow of Institute for Material Research in Tohoku University. In 2000–2004, he was a visiting scholar in Physics Department of the Hong Kong University of Science and Technology. He is currently a "Xi-De" chair professor in Physics Department of Fudan University. His working fields include metamaterials, photonic crystals and plasmonics.